International Journal of Minerals, Metallurgy and Materials
Volume 27, Number 11, November 2020, Page 1517
https://doi.org/10.1007/s12613-020-2001-8

Influence of welding speed on microstructure formation in friction-stir-welded 304 austenitic stainless steels

Mohsen Hajizadeh[1*], *Sajjad Emami*[2*], *and Tohid Saeid*[2)]

1) Faculty of Mechanical Engineering, Sahand University of Technology, Tabriz, Iran
2) Faculty of Materials Engineering, Sahand University of Technology, Tabriz, Iran
(Received: 18 October 2019; revised: 21 January 2020; accepted: 5 February 2020)

Abstract: The influence of welding speed on the joint microstructures of an austenitic stainless steel (ASS) produced by friction stir welding (FSW) was investigated. The FSW process was conducted using a rotational speed of 400 r/min and welding speeds of 50 and 150 mm/min. The study was carried out using electron backscattered diffraction (EBSD) technique in different regions of the resultant stir zones (SZs). The results show that the texture of the advancing side (AS) was mainly composed of C {001}⟨110⟩ and cube {001}⟨100⟩ texture components along with partial B/$\bar{\text{B}}$ {112}⟨110⟩ component. Moving from the AS toward the center and the retreating side (RS), the cube texture component disappeared and the A_1^*/A_2^* {111}⟨112⟩ component developed and predominated the other components. Higher welding speed greatly affected and decreased the intensity of the textures in the resultant SZs. Moreover, higher welding speed (lower heat input) resulted in lower frequency of cube texture in the AS.

Keywords: friction stir welding; stainless steels; welding speed; dynamic recovery; shear texture; continuous dynamic recrystallization

1. Introduction

Austenitic stainless steels (ASS) are considered as one of the important class of engineering materials that are widely used in many different industrial applications [1–4]. The friction-stir welding (FSW) of such high melting point materials have been the case study of many scientists in recent years. Due to its solid state nature, FSW can effectively reduce the common problems associated with traditional welding techniques, such as the occurrence of solidification cracking and coarse dendritic structure in the fusion zone and stress corrosion cracking and weld decay in the heat-affected zone (HAZ) of ASS [1,5]. Friction stir welding utilizes the heat and the deformation to produce a joint [5–6]. The joints are usually produced along with simple shear texture components [7]. The development of textural components results in anisotropy through the microstructure of the welded material and finally affects the mechanical behavior of the welded material [8]. The simple shear texture components that occur through the microstructure of the processed face-centered cubic (fcc) metals include A/$\bar{\text{A}}$ {111}⟨110⟩, A_1^*/A_2^* {111}⟨112⟩, B/$\bar{\text{B}}$ {112}⟨110⟩, and C {001}⟨110⟩ [7]. The occurrence of each component and its contributions are determined by the Taylor factor [9]. Therefore, different deformational conditions result in the activation of different slip systems, which in turn causes the formation of different textural components. Considering the nature of the FSW, the material receives different amount of temperature, strain, and strain rate throughout the welded region, and different texture components develop accordingly. Therefore, temperature, strain, and strain rate are the most important factors affecting the thermo-mechanically activated processes, such as the activation of different slip systems, dynamic recovery, and recrystallization through the microstructure [10]. It has been well reported that in the FSW process, the heat generation is mainly linked to the material flow [5–6], and in reports on textural studies, temperature is not treated as an independent variable [11–12]. However, the temperature slightly differs in different regions of the stir zone (SZ), including the advancing side (AS), center, and retreating side (RS). The temperature can be neglected in textural studies, since the magnitude of strain and the strain rate change in the same path, and their amounts change as the deformation condition changes; therefore, their combinations might act differently

*These authors contributed equally to this work.
Corresponding author: Tohid Saeid E-mail: saeid@sut.ac.ir

in different regions of the SZ. In this regard, several attempts of FSW application on austenitic stainless steels (ASSs) have been made [13–20]. The early studies were limited to the possibility of FSW on such materials. For example, Meran *et al*. [13] studied the feasibility of FSW on a 304 ASS. Reynolds *et al*. [14] investigated the resultant joint characteristics including mechanical properties and residual stress of an FS-welded 304L ASS. However, recent investigations are mainly about the microstructure formation during the FSW process. Park *et al*. [15] and Meran and Canyurt [16] investigated the occurrence of dynamic recrystallization (DRX) through the microstructure of an FS-welded 304 ASS without identifying the type the DRX. Sato *et al*. [17] investigated the FS-welded joints of a 304L ASS and indicated that a very fine and recrystallized grain structure developed in the microstructure of the SZ along with a <100> fiber texture component. Rezaei-Nejad *et al*. [18] studied the microstructural changes in a friction stir-processed 316L ASS and reported the occurrence of discontinuous dynamic recrystallization (DDRX) as a predominant operating mechanism in the formation of the SZ microstructure. Hajian *et al*. [19] conducted friction stir processing on a 316L ASS using electron backscattered diffraction (EBSD) technique and transmission electron microscopy (TEM). They reported the occurrence of DDRX as a responsible mechanism in the microstructure formation exhibiting a high fraction of dislocations in the SZ. These researchers also mentioned that partial continuous dynamic recrystallization (CDRX) occurred in the SZ. They showed the presence of subgrains that tended to absorb lattice dislocations and increased their misorientation angle. Liu and Nelson [20] studied the evolution of grain structure and the texture of a 304L ASS introduced in FSW joints. They found that the microstructure formation occurred mainly through DDRX mechanism due to grain boundary bulging and migration. Emami and Saeid [21] conducted FSW on a 304 ASS with a different welding parameter (400 r/min, 50 mm/min). They found that the microstructure evolved mainly through the occurrence of CDRX and partially through DDRX.

The literature survey reveals that all the previous works focused on a fixed parameter, and the influence of the deformation condition has not been investigated so far. In the current study, the authors investigate the effect of two different welding speeds on the development of microstructure in different regions of the resultant SZs.

2. Experimental

The material used in this study was an AISI 304 ASS plate with 2 mm thickness. Bead-on-plate FS welds were applied on the prepared 100 mm × 100 mm specimen. Based on previous works [21–23], the welding was conducted along the rolling direction of the prepared samples at a constant rotational speed of 400 r/min and welding speeds of 50 and 150 mm/min. Moreover, temperature measurements reported for FS-welded SAF 2205 duplex 2 mm thick plates have shown that the temperature significantly decreased with increase in welding speeds from 50 mm/min to 150 mm/min and at a constant rotational speed of 600 r/min [22]. Therefore, the difference in temperature is estimated to be more significant at a rotational speed of 400 r/min. A WC-based alloy was used to design the welding tool, with its pin having a conical geometry. The tool shoulder, pin base, pin tip diameters, and pin height were 16, 4.5, 3.5, and 1.7 mm, respectively. During the welding procedure, the depth of the pin penetration into the sample was kept constant at 1.8 mm. To keep parameters such as plunge depth and tool vertical force unchanged, the welding was started with 50 mm/min and continued with 150 mm/min without any tool pullout. Microstructural observations were mainly conducted along the normal direction–transverse direction (ND-TD) of the cross section, using a scanning electron microscope equipped with an EBSD analysis system. The EBSD data were obtained from the cross section, which was perpendicular to the welding direction. The EBSD specimens were mechanically pre-polished with 1 and 0.25 μm diamond pastes, electro-polished with a solution of 700 mL ethanol, 120 mL distilled water, 100 mL glycerol, and 80 mL perchloric acid at ambient temperature and a voltage of 35 V for 10 s. Electron backscattered diffraction analyses using orientation mapping and orientation distribution function (ODF) were performed according to the methodology described in the previous works [23–24].

3. Result and discussion

3.1. Base Metal

Fig. 1 displays the results of EBSD analysis on the ND-TD cross section of a welded sample. Crystal orientation and grain boundary maps (Figs. 1(a) and 1(b)) show that the base metal (BM) microstructure included an equiaxed grain structure. The misorientation angle histogram is similar to that of a randomly oriented material; however, a very intense peak occurs at 60°. The presence of this peak is related to the formation of coincidence site lattices (CSLs). The misorientation angle/axis pairs in the misorientation angle histogram show that the main fractions of the CSL boundaries are distinguished to have a first-order relationship defined by a 60° rotation about <111> axis. It has been reported that the CSL boundaries are generally generated in the recrystallized microstructure of fcc-structured materials during the grain growth phenomenon [21,23–24]. The results from statistical analysis of the grain boundaries (grain boundary character distribution (GBCD) diagrams) also reveal that the grain boundaries were mainly composed of main grain boundaries known as high-angle grain boundaries (HAGB) and CSLs,

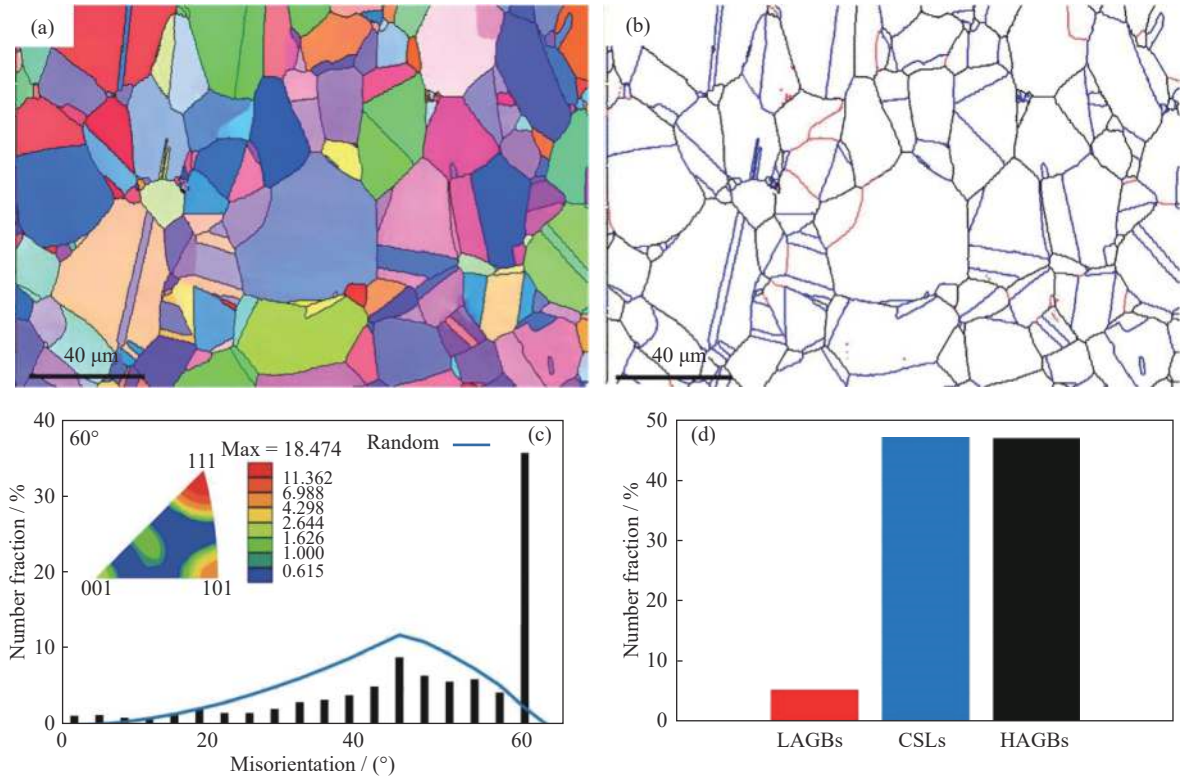

Fig. 1. EBSD data from the BMs: (a) crystal orientation map, (b) grain boundary map, (c) misorientation angle histogram, and (d) grain boundary characterization distribution.

which implies that the initial microstructure had gone through an annealing process. Stacking fault energy (SFE) is one of the main determining factors in the formation of CSLs; that is, a low SFE helps the formation of annealing twining and CSLs [21]. Therefore, austenitic stainless steels with rather low SFEs are more prone to develop such boundaries during deformation at high temperatures.

3.2. Thermo-mechanically affected zone

Fig. 2 shows the EBSD data obtained from the ND-TD cross section of the thermo-mechanically affected zones (TMAZs) at different welding speeds. The resultant microstructures show that the FSW severely deformed and elongated the constituent grains of the TMAZs with respect to the stress imposed through the stirring action of the welding tool. Misorientation angle histogram (Fig. 2(e)) shows that high fraction of LAGBs was developed in the TMAZs. Such boundaries have been reported to be formed in the TMAZ of FS-welded materials through the occurrence of dynamic recovery process [21–24]. During the deformation at high temperature, a certain number of mobile dislocations is necessary in order to accommodate the strain and strain rate. Therefore, during the welding procedure, new dislocations are introduced in the microstructure of the evolved material. These dislocations start to interact with each other and those with opposite signs are effectively eliminated at the welding temperature. After the elimination, only one type of dislocations is left in the material, and the dislocations tend to rearrange themselves into low-angle grain boundaries (LAGBs) and form sub-structures; this process is known as dynamic recovery process.

It is also shown that the fraction of LAGBs in the TMAZ of the sample welded with 150 mm/min was higher than that of the sample welded with 50 mm/min. This behavior is attributed to the degree of deformation imposed by the welding tool, which was higher for the sample welded with 150 mm/min. As the deformation degree increased, the density of dislocations also increased; therefore, the activation energy for processes such as dislocation slips and climbs, which are necessary for softening mechanisms, increased [10]. Comparing the GBCDs of the BM and the TMAZ reveals that the frequency of the CSL boundaries decreased from the BM toward the TMAZ. It seems that the stirring action of the welding tool affected the orientation of the CSLs and caused them to deviate from their ideal relationship [20–21].

3.3. Stir zone

Fig. 3 depicts the grain boundary maps along with misorientation angle histograms from different regions of SZs. This figure demonstrates that the deformed grain structure of the TMAZ (Fig. 2) was replaced by a fine equiaxed and recrystallized structure in the SZs. The relationship between severe deformation and high temperature leads to the development of very fine equiaxed microstructures in the SZs through the

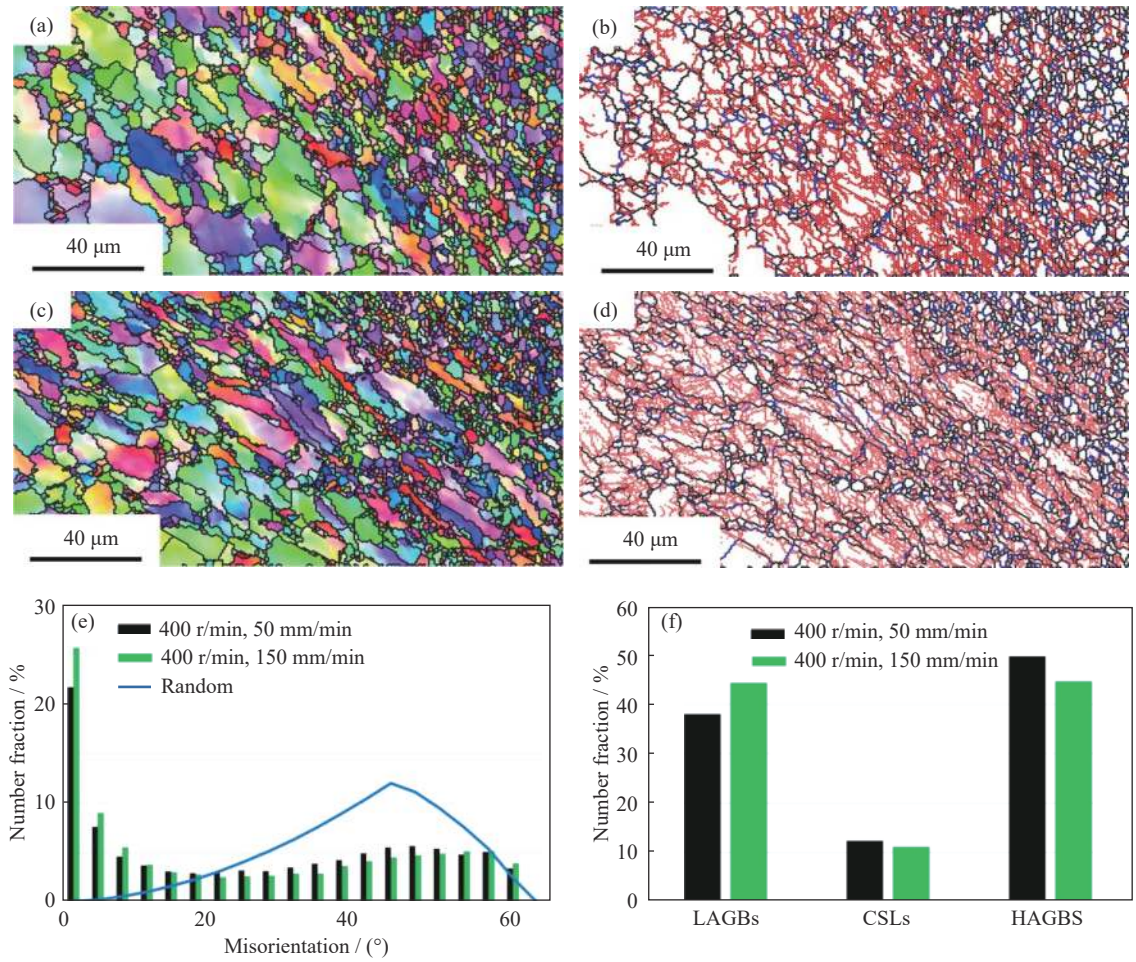

Fig. 2. EBSD data from the TMAZs: (a) crystal orientation map for a welding speed of 50 mm/min; (b) grain boundary map for a welding speed of 50 mm/min; (c) crystal orientation map for a welding speed of 150 mm/min; (d) grain boundary map for a welding speed of 150 mm/min; (e) misorientation angle histogram; (f) grain boundary characterization distribution.

DRX phenomenon [21,23]. The figure also shows that coarser grains were developed in the SZ of the material welded with low welding speed. This is probably due to the amount of generated heat during welding procedure. Since the heat generated during FSW is inversely proportion to the welding speed, the average grain size of the SZ is increased with a decrease in the welding speed, and the SZ resulting from the low welding speed was subjected to a high temperature, which in turn resulted in a coarse microstructure [5–6]. Fig. 4 depicts the statistical analysis from the grain boundaries. The number of LAGBs decreased from the AS toward the RS of the resultant SZs. This is more likely related to the contribution of the applied deformation and the temperature. Based on the asymmetric nature of the FSW in the AS, where the material receives a higher degree of temperature and deformation, phenomena such as dislocation climbs and slips can easily be activated, leading to the formation of a large number of LAGBs [1,10]. On the other hand, it is seen that the number of CSLs increased in the same path from AS toward the RS. As the applied stress decreases from the AS toward the RS, the stirring action of the tool can rotate away and cause few CSLs to deviate.

Fig. 5 shows the texture of the BM representing the ODF sections along with the standard textural components of rolled fcc materials. The ODF sections show that the texture of the starting material is mainly composed of the textural components of S {123}<634> ($\varphi_1 = 59°$, $\Phi = 37°$, $\varphi_2 = 63°$), C {112}<111> ($\varphi_1 = 90°$, $\Phi = 35°$, $\varphi_2 = 45°$), B {011}<211> ($\varphi_1 = 35°$, $\Phi = 45°$, $\varphi_2 = 90°$), G {011}<100> ($\varphi_1 = 0°$, $\Phi = 45°$, $\varphi_2 = 90°$), and cube {001}<100> ($\varphi_1 = 0°$, $\Phi = 0°$, $\varphi_2 = 0°$). Among these textural components, B and C have been reported to form during the rolling process, while S, G, and cube have been reported to develop during recrystallization process [10]. Moreover, the formation of recrystallization textural components has been reported to reduce the intensity of the deformational texture and randomize it. Therefore, S, G, and cube might be related to the recrystallization phenomenon, which effectively reduced the intensity of the BM texture.

Figs. 6 and 7 show the results of texture analysis from the

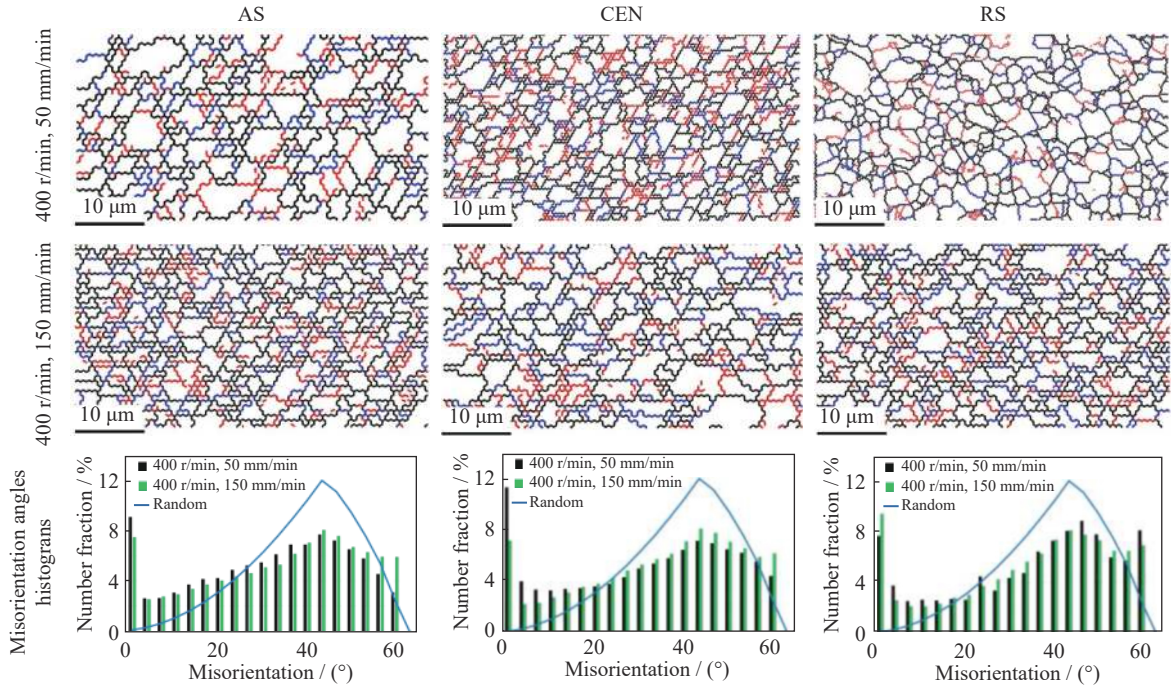

Fig. 3. EBSD data from different regions of resultant SZs (AS, CEN, and RS correspond to advancing side, center, and retreating side of the SZ, respectively).

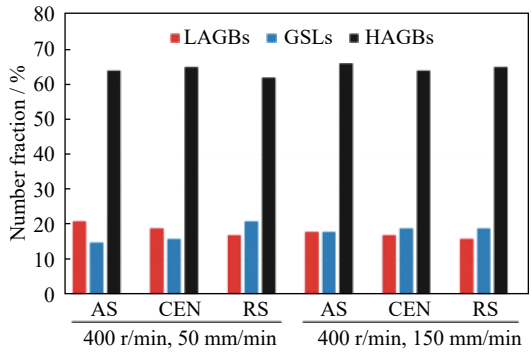

Fig. 4. Grain boundary character distribution of the resultant SZs.

centerline of the resultant SZs. Pole figures {111} and {110} show that a simple shear texture was introduced through the SZs microstructure. Shear textures are generally represented by the sample coordinate system of {shear plane (SP)}<shear direction (SD)>, associated with the crystal coordinate system of {*hkl*}<*uvw*> [25–26]. The common fcc slip system is {111}<110>, which can be described as {111}//SP and <110>//SD [20–23]. It is also clear from Fig. 6 that intensities of the resultant pole figures decrease from the AS, where the material received a high magnitude of temperature and deformation with respect to the center and the RS [24]. This behavior indicates the existence of strain gradient in the SZs.

As indicated in Fig. 6, the positions of the ideal simple shear textures are very close to each other in the pole figures and might be overlapping. Therefore, to carefully investigate the texture, ODFs were calculated to avoid any interference. Fig. 7 depicts the resultant ODFs from the AS, center, and the RS of the SZ, at $\varphi_2 = 0°$ and $\varphi_2 = 45°$. The ideal simple shear texture components for fcc materials are also presented in Fig. 7. The ODF sections also confirm the presence of a simple shear texture in the SZ. The results show that the texture of the AS was mainly composed of C {001}<110> and cube {001}<100> texture components along with partial B {112}<110> component. The components C and B have been well reported to occur throughout the microstructure of a processed fcc material in simple shear deforming technique [21], whereas the cube texture usually occurs through the microstructure of a recrystallized materials. It can be seen from

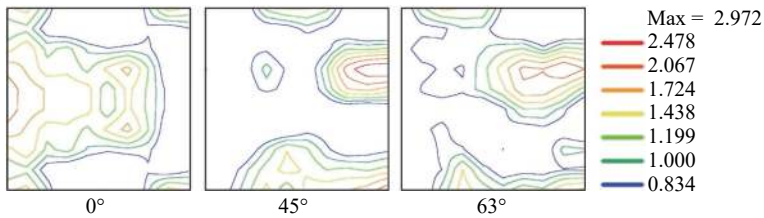

Fig. 5. Texture of the BM represented with ODF sections.

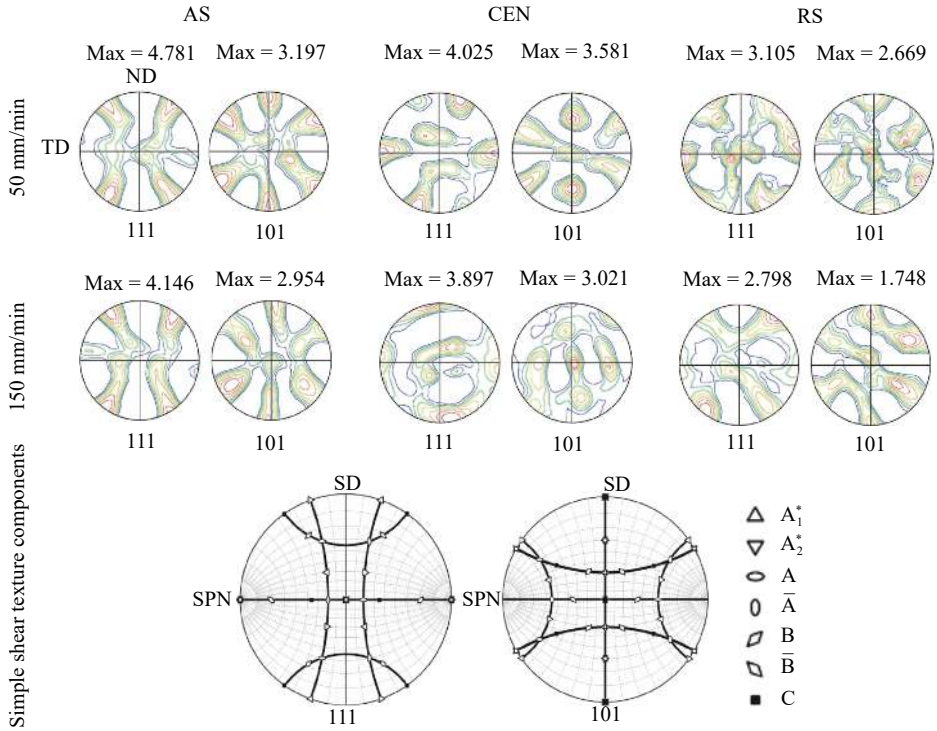

Fig. 6. {111} and {110} pole figures obtained from different regions of the SZs along with the positions of the ideal simple shear texture components; SPN and SD are oriented as shown.

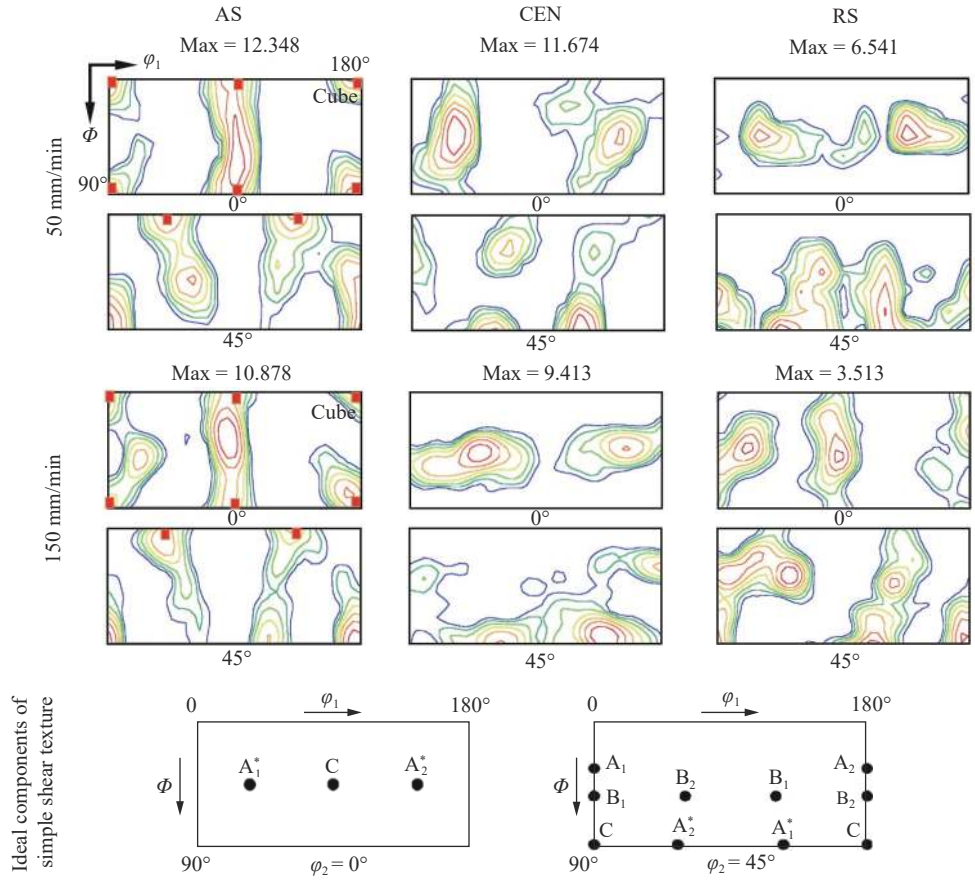

Fig. 7. ODF sections obtained from different regions of the SZs at different welding speeds along withthe locations of the ideal components of simple shear texture in the fcc metals.

the ODF sections that the cube texture was developed in the AS for both welding speeds. The cube texture formation for both welding speeds is more likely due to the amount of heat generated in the region. For the AS, where the welding and rotational speeds are of the same direction, the applied strains from the advancing force and the rotational force strengthen each other, and the material receives higher amount of heat. Therefore, the material in the AS receives a high temperature, which results in the occurrence of static and/or discontinuous DRX. It can be seen that the intensity of the texture in the AS tended to decrease with increasing welding speed. This behavior implies that the rotational speed has a very significant influence on the development of simple shear textures, which decrease by increasing the welding speed. The ODF sections apparently show that the textural components of C, B, and cube were replaced by A_1^*/A_2^* $\{111\}\langle 112\rangle$ and $B/\bar{B}$ $\{112\}\langle 110\rangle$ running from AS toward the center and the RS of the resultant SZs. Moreover, the intensity of the texture decreased in the same path. However, the reason for the change in the textural components has not been fully determined thus far [11–12,25]; it is the strain, strain rate, and temperature that have been discovered to affect the hot deformation behavior of the processed material in the FSW [26]. Further crystal orientation maps from the AS of the resultant SZs in Fig. 8 qualitatively show that the frequency of cube texture component decreased as the welding speed increased. This is probably due to the amount of heat generated in the SZs. The SZ welded with low welding speed (higher heat input) resulted in the formation of a higher number of grains with cube texture components compared with the sample welded with high welding speed.

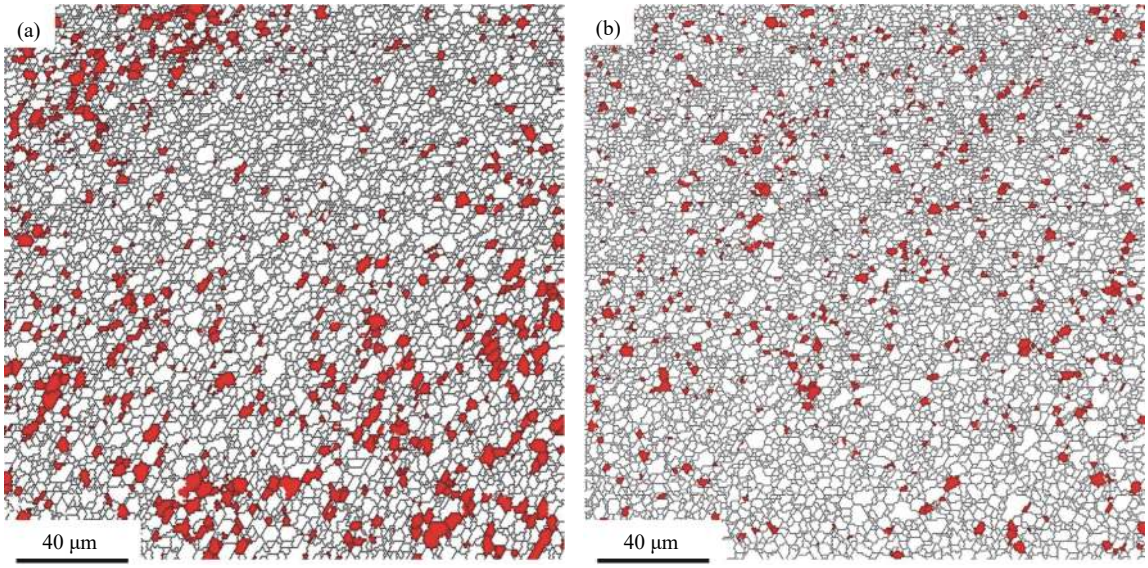

Fig. 8. Crystal orientation maps from the AS of the SZs indicating the frequency cube texture component: (a) 50 mm/min; (b) 150 mm/min.

4. Conclusion

The microstructural changes of a friction-stir-welded AISI 304 austenitic stainless steel were evaluated using EBSD. The results revealed that very fine microstructures associated with simple shear textures were developed in the stir zone of the produced joints. The ASs of the stir zones also experienced static and/or discontinuous DRXs and developed a cube $\{001\}\langle 100\rangle$ recrystallization texture component. It was found that the cube texture disappeared moving from the AS toward the center and the retreating side. The simple shear texture component of A_1^*/A_2^* $\{111\}\langle 112\rangle$ also developed in the center and the retreating side. In addition, it was observed that with increasing welding speed from 50 to 150 mm/min, due to lower heat generation, finer grains were formed in the SZ. On the other hand, the frequency of cube texture component decreased as the welding speed increased.

References

[1] S.H.C. Park, Y.S. Sato, H. Kokawa, K. Okamoto, S. Hirano, and M. Inagaki, Microstructural characterisation of stir zone containing residual ferrite in friction stir welded 304 austenitic stainless steel, *Sci. Technol. Weld. Joining*, 10(2005), No. 5, p. 550.

[2] A. Marchattiwar, A. Sarkar, J.K. Chakravartty, and B.P. Kashyap, Dynamic recrystallization during hot deformation of 304 austenitic stainless steel, *J. Mater. Eng. Perform.*, 22(2013), No. 8, p. 2168.

[3] Sindo Kou, *Welding Metallurgy*, 2nd ed., John Wiley & Sons Publication, New Jersey, 2003.

[4] S. Tokita, T. Yokoyama, H. Kokawa, Y.S Sato, and H.T Fujii, Friction stir welding of grain boundary engineered 304 austenitic stainless steel, [in] *Proceedings of the 1st International Joint*

Symposium on Joining and Welding, Osaka, 2013, p. 407.
[5] R.S. Mishra and Z.Y. Ma, Friction stir welding and processing, *Mater. Sci. Eng. R*, 50(2005), No. 1-2, p. 1.
[6] R.S. Mishra, P.S. De, and N. Kumar, *Friction Stir Welding and Processing, Springer*, Switzerland, 2014.
[7] R.W. Fonda and K.E. Knipling, Texture development in friction stir welds, *Sci. Technol. Weld. Joining*, 16(2011), No. 4, p. 288.
[8] Z.H. Zhang, W.Y. Li, J.L. Li, Y.J. Chao, and A. Vairis, Microstructure and anisotropic mechanical behavior of friction stir welded AA2024 alloy sheets, *Mater. Charact.*, 107(2015), p. 112.
[9] P. Ghosh, O. Renk, and R. Pippan, Microtexture analysis of restoration mechanisms during high pressure torsion of pure nickel, *Mater. Sci. Eng. A*, 684(2017), p. 101.
[10] F.J. Humphreys and M. Hatherly, *Recrystallization and Related Annealing Phenomena*, 2nd ed., Elsevier, Oxford, 2004.
[11] S. Mironov, K. Inagaki, Y.S. Sato, and H. Kokawa, Effect of welding temperature on microstructure of friction-stir welded aluminum alloy 1050, *Metall. Mater. Trans. A*, 46(2015), p. 783.
[12] S. Mironov, K. Inagaki, Y.S. Sato, and H. Kokawa, Microstructural evolution of pure copper during friction-stir welding, *Philos. Mag.*, 95(2015), No. 4, p. 367.
[13] C. Meran, V. Kovan, and A. Alptekin, Friction stir welding of AISI 304 austenitic stainless steel, *Materialwiss. Werkstofftech.*, 38(2007), No. 10, p. 829.
[14] A.P. Reynolds, W. Tang, T. Gnaupel-Herold, and H. Prask, Structure, properties, and residual stress of 304L stainless steel friction stir welds, *Scripta Mater.*, 48(2003), No. 9, p. 1289.
[15] S.H.C. Park, Y.S Sato, H. Kokawa, K. Okamoto, S. Hirano, and M. Inagaki, Rapid formation of the sigma phase in 304 stainless steel during friction stir welding, *Scripta Mater.*, 49(2003), No. 12, p. 1175.
[16] C. Meran and O.E. Canyurt, Friction stir welding of austenitic stainless steels, *J. Achiev. Mater. Manuf. Eng.*, 43(2010), No. 1, p. 432.
[17] Y.S. Sato, T.W. Nelson, and C.J. Sterling, Recrystallization in type 304L stainless steel during friction stirring, *Acta Mater.*, 53(2005), No. 3, p. 637.
[18] S.S. Rezaei-Nejad, A. Abdollah-zadeh, M. Hajian, F. Kargar, and R. Seraj, Formation of nanostructure in AISI 316L austenitic stainless steel by friction stir processing, *Procedia Mater. Sci.*, 11(2015), p. 397.
[19] M. Hajian, A. Abdollah-zadeh, S.S. Rezaei-Nejad, H. Assadi, S.M.M. Hadavi, K. Chung, and M. Shokouhimehr, Microstructure and mechanical properties of friction stir processed AISI 316L stainless steel, *Mater. Des.*, 67(2015), p. 82.
[20] F.C. Liu and T.W. Nelson, *In-situ* grain structure and texture evolution during friction stir welding of austenite stainless steel, *Mater. Des.*, 115(2017), p. 467.
[21] S. Emami and T. Saeid, A comparative study on the microstructure development of friction stir welded 304 austenitic, 430 ferritic, and 2205 duplex stainless steels, *Mater. Chem. Phys.*, 237(2019), art. No. 121833.
[22] T. Saeid, A. Abdollah-zadeh, H. Assadi, and F. Malek Ghaini, Effect of friction stir welding speed on the microstructure and mechanical properties of a duplex stainless steel, *Mater. Sci. Eng. A*, 496(2008), No. 1-2, p. 262.
[23] T. Saeid, A. Abdollah-zadeha, T. Shibayanagi, K. Ikeuchi, and H. Assadi, On the formation of grain structure during friction stir welding of duplex stainless steel, *Mater. Sci. Eng. A*, 527(2010), No. 24-25, p. 6484.
[24] S. Emami, T. Saeid, and R.A. Khosroshahi, Microstructural evolution of friction stir welded SAF 2205 duplex stainless steel, *J. Alloys Compd.*, 739(2018), p. 678.
[25] M.M.Z. Ahmed, B.P. Wynne, M.M.El-Sayed Seleman, and W.M. Rainforth, A comparison of crystallographic texture and grain structure development in aluminum generated by friction stir welding and high strain torsion, *Mater. Des.*, 103(2016), p. 259.
[26] X.C. Liu, Y.F. Sun, T. Nagira, K. Ushioda, and H. Fujii, Strain rate dependent micro-texture evolution in friction stir welding of copper, *Materialia*, 6(2019), art. No. 100302.